Industrial Scale Engineering of Photocatalytic Nanomaterials by Flame Spray Pyrolysis (F.S.P.)

Areti Zindrou[1, a], Asterios Mantzanis[1, b] and Yiannis Deligiannakis[1, c, *]

[1]Laboratory of Physical Chemistry of Materials & Environment, Department of Physics, University of Ioannina, Ioannina, Greece

[a]a.zindrou@uoi.gr, [b]a.mantzanis@uoi.gr, [c]ideligia@uoi.gr

Keywords: Photocatalysis, Artificial Photosynthesis, Water-splitting, H_2, O_2, Doping, Flame Spray Pyrolysis, Industrial Engineering, Nanomaterials, $BiVO_4$, TiO_2.

Abstract. Flame Spray Pyrolysis is an attractive technology for the synthesis of nanosized materials with distinct characteristics. Industry leaders such as Cabot, Cristal, DuPont, Evonik, and Ishihara manufacture flame-made materials in millions of tons per year including carbon blacks. Herein we exemplify the application of large-scale FSP process for the synthesis of highly active photocatalysts, able to achieve high H_2, O2 production yields from H_2O. Precise control of W-doping along with controlled Scheelite-phase $BiVO_4$ is a benchmark oxygen-evolving nano-catalyst. Double-Nozzle FSP is demonstrated to allow the production of highly efficient {noble metal} TiO_2 heterostructures. Key-Performance-Indicators that allow transition of Lab-Scale to Industrial-Scale engineering of semiconductors are discussed, including cost-analysis and environmental impact of the production process.

Introduction

Engineering nano-photosynthetic systems to efficiently convert the abundant solar energy into chemical fuels in accordance with global energy demands is of utmost importance and brings us a step closer to a sustainable and carbon-neutral society. Powder-like semiconducting photocatalysts, ever since Fujishima and Honda[1], have been in the spotlight in the last 50 years finding applications in CO2 reduction[2], pollutants removal[3], and in H_2 production from water splitting or photo-reformation of H2O/alcohol (i.e., methanol and ethanol) mixtures[4]. For a semiconductor to be considered as a successful nano photocatalyst one must design materials with controlled characteristics (i.e., chemical composition, size, phase, defects). In particular, metal oxides with proper conduction band (CB) and valence band (VB) potentials as well as with an energy gap (Eg) in the visible or UV region can perform successfully the above-mentioned photocatalytic reactions[5].

In this context, large-scale production of nanoparticles by flame aerosol technique has a significant contribution in the progress of nanotechnology. Industry leaders such as Cabot, Cristal, DuPont, Evonik, and Ishihara manufacture flame-made materials in millions of tons per year including carbon blacks, the widely known photocatalytic TiO_2 P25 by Evonik[6], fumed SiO_2, Al_2O_3, and other ceramic nanoparticles finding application as pigments[7], reinforcing agents[8] and flowing aids[9]. Besides plain metal oxides, mixed metal oxide systems ($V_2O_5/WO_3/TiO_2$[10], $Cu/ZnO/Al_2O_3$[11], Co_3O_4/CoO[12]), perovskites ($LaBO_3$ (B=Co,Mn)[13], $SrTiO_3$[14], YSZ[15], $BiFeO_3$, $Bi_2Fe_4O_9$[16,17]) as well as oxide supported noble metals (Pt/Al_2O_3[15], $Pt/CeZrO_2$[18]) have already been made using flame aerosol technology. Flame aerosol synthesis has many appealing features that are not feasible with wet-chemistry methods, the most important difference between them is the number of steps involved. Generally, wet-chemistry methods involve many time-consuming steps whilst flame methods favor rapid one-step synthesis. Moreover, catalysts prepared through flame aerosol process rarely require post thermal treatment due to the *in-situ* calcination during the high-temperature synthesis. Flame synthesis allows continuous production, while wet-chemistry methods are batch processes. Nevertheless, as appealing flame aerosol process may sound there are some limitations, including the selection of suitable precursors and their cost as well as their mixability. Moreover, one should also consider the potentially hazardous, explosive

conditions and precursor mixtures that may arise, and, in some cases, there might be uncombusted products on the final material. However, the ever-growing needs of the market demand more complex and functional materials the scalability of which remains yet a challenge.

Thus, the aims of the present work were: [i] the production of W-doped $BiVO_4$ nanoparticles with controlled O-vacancies using FSP[19] and [ii] the production of TiO_2 nanocatalysts decorated with controllable amount of noble metal particles [NM^0 = Pt^0, Pd^0, Au^0, Ag^0][20] and their potential applications in O_2 and H_2 production from H_2O respectively. Specifically, in the case of TiO_2, we focus on the comparison of photocatalytic performance of nanocatalysts synthesized by two FSP methods.

F.S.P. Synthesis of Nanocatalysts

Flame Spray Pyrolysis (F.S.P.) is a versatile and scalable process allowing the formation of metastable phases and thus catalytic materials with tunable characteristics such as specific surface area (SSA), particle size, and crystallinity through its process parameters[9]. Compared to wet-chemical processes involving many post-treatment steps (e.g., filtration, washing, drying, calcination), flame aerosol allows the synthesis of the desired material without further post-treatment.

Even though this method was envisioned by Ulrich [21] at 1971 and developed at 1977 by Sokolowski et al. for the synthesis of Al_2O_3[22], it took many years until researchers employ this technique for the synthesis of nanoparticles [23,24]. In an FSP process, the selection of precursors and solvents with suitable combustion enthalpies, melting/decomposition temperatures, and chemical stability is crucial to the overall particle formation [24]. The highly exothermic nature of FSP liquid precursors and the high gas velocities coupled with the radiation heat loss give rise to extremely short residence times (milliseconds) with high-temperature gradients along the flame axis[25]. This interplay between high temperature and the large temperature gradient is one of the most important features in FSP. Due to these high local temperatures, highly crystalline and homogeneous materials are produced[9]. Furthermore, flame spraying in open ambient air conditions provides a continuous O2 supply to the flame during particle synthesis resulting in materials with minimal amounts of carbon soot, also rendering particles with high thermal stability compared to other lower temperature techniques. It should be noted that the formation of mixed metal oxides and perovskites is favored in single nozzle systems due to the homogeneous distribution of the precursor components and the facilitation of ion diffusion[26].

Double-Nozzle Flame Spray Pyrolysis (or double-nozzle) (Fig. 1c) is a variation of the FSP process, and it involves the use of two nozzles to produce the end product. It builds upon the success of the traditional FSP process and provides a platform to circumvent its shortcomings. Two nozzles can be employed, concurrently producing metal oxides doped with metal hetero-atoms[27]. This is the primary advantage against the traditional FSP process. Catalytic reactions are surface reactions i.e., they take place at the catalyst's surface. Doping with traditional FSP leads to the non-homogeneous, both in the bulk and at the surface, dispersion of dopants. By adding an additional nozzle, we are essentially adding two additional degrees of freedom (inter-nozzle distance and nozzle-to-nozzle degree). This leads to the homogenous surface dispersion of metal dopants. Furthermore, by proper engineering of the two additional degrees of freedom, we can make sure that the droplets from the second nozzle have already formed particles once they come into contact with the product from the first nozzle. This modified process has already been used for the synthesis of $CoMo/Al_2O_3$[28] hydrotreating catalysts, alumina supported cobalt[29] Fischer-Tropsch catalysts, $MnOx/\gamma\text{-}Al_2O_3$ and $FeOx/\gamma\text{-}Al_2O3$[30] for CO removal, La-doped Co/Al_2O_3[31], and SiO_2/CZO[32] for dry reforming of methane.

In FSP the metal precursor is fed at the center of the reactor with the aid of a syringe pump, then is dispersed by gas convection through a nozzle forming a spray which is ignited[33]. The metal precursor evaporates to precursor vapor leading to the generation of the primary particles which subsequently form stable agglomerates and finally we collect them in powder form. Some of the most important parameters we must take into consideration that affect product properties and specifically the primary particle are precursor concentration, precursor/dispersion flow rate ratio (P/D), precursor

solution composition, fuel, and air entrainment to name a few[26]. Moreover, regarding catalytic processes, there are some particle properties that can affect the final result such as the chemical composition which is a key parameter in the design of catalysts, particle size, and shape which can increase the number of active sites improving the overall catalytic performance and specific surface area which affects many catalytic reactions. FSP synthesis is considered ideal for the synthesis of metastable phases and crystal structures or high SSA materials with controlled phase composition.

Taking into consideration all of the above-mentioned FSP characteristics, we present two experimental setups for the successful synthesis of W-doped $BiVO_4$ (Fig. 1a) and TiO_2 nanocatalysts decorated with controllable amounts of noble metals (Fig. 1b and 1c). The produced nanopowders were evaluated for the photocatalytic evolution of O_2 and H_2 by H_2O respectively. Especially, in the case of TiO_2, we have synthesized a series of noble metal decorated TiO2 nanocatalysts using both one-nozzle FSP (ON-FSP) and double-nozzle FSP (DN-FSP) in order to obtain the desired NM^0/TiO_2 nano-hybrids (Fig. 1b and 1c).

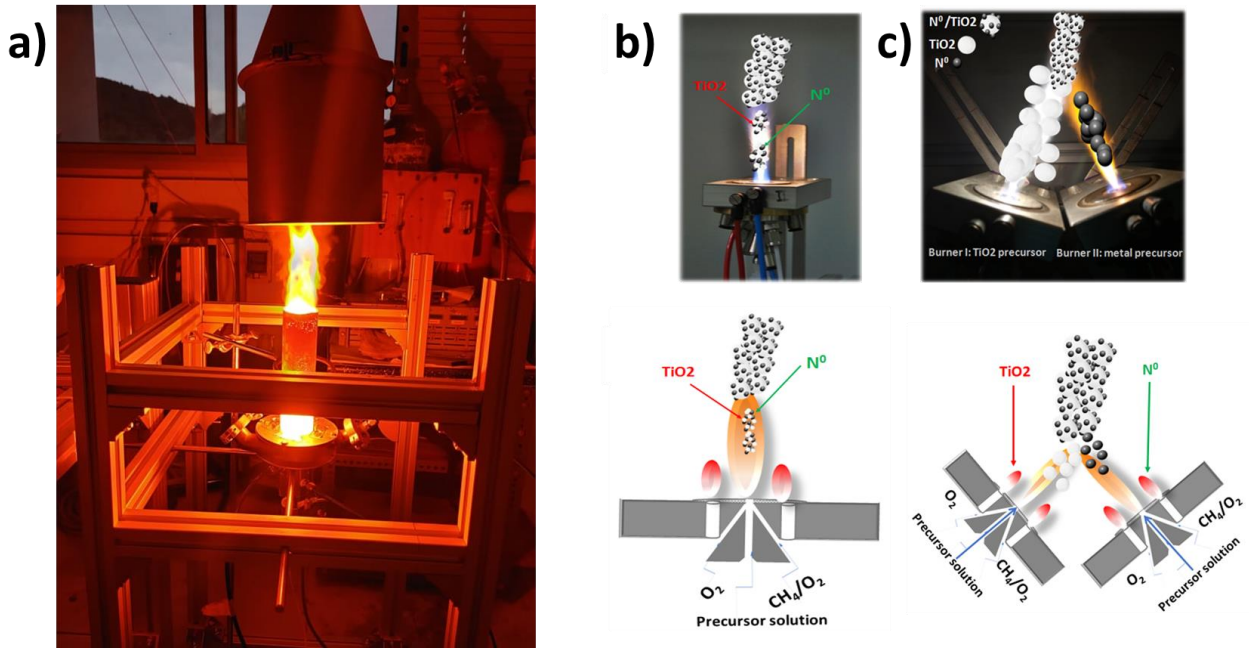

Figure 1. Our Flame Spray Pyrolysis (FSP) set-up: **a)** Enclosed reactor to produce highly crystalline W-doped $BiVO_4$ nanocatalysts; **b)** One Nozzle-FSP where TiO_2 and NM^0= Pt^0, Pd^0, Au^0, Ag^0 are formed in the same nozzle; **c)** Double-Nozzle FSP. Burner-1 was used for the formation of TiO_2-nanoparticles while Burner-2 was dedicated to the formation of noble metal.

Results

The X-ray diffraction patterns of the FSP-made W-doped $BiVO_4$ nanoparticles are presented in Fig. 2a. Generally, the W-doping cause rather minor changes in particle size, and there is no indication or diffraction peaks from secondary oxide phases such as WO_3. Moreover, W-doping has no effect on the peak positions neither $BiVO_4$ phase-change (i.e., from monoclinic to tetragonal phase) (Fig. 2a). It is safe to say W-doping does not affect the crystal structure of $BiVO_4$ and we attribute this to the comparable atomic radius of Bi and W-atoms which play an essential role in the stabilization of the crystal structure. The photocatalytic O_2 evolution was investigated using Au as a co-catalyst to collect the photogenerated electrons. Comparing 5W-$BiVO_4$ with the pristine $BiVO_4$ we observe a 270% higher activity under the same photocatalytic conditions (Fig. 2b).

Regarding the NM^0-TiO_2 materials, X-ray diffraction profiles are shown in Fig 3a and 3b for ON-FSP and DN-FSP with NM^0 loading 0.5% N^0/TiO_2. Generally, no differences were observed in the XRD patterns of TiO_2 among the different noble-metal deposits and no XRD diffraction peak of any noble metal was resolved indicating that the noble metal particle sizes were < 2nm. Under the same

photocatalytic conditions and the noble metal loading, the performance in H_2 production follows the trend

$$Pt>Pd>Au>Ag \qquad (1)$$

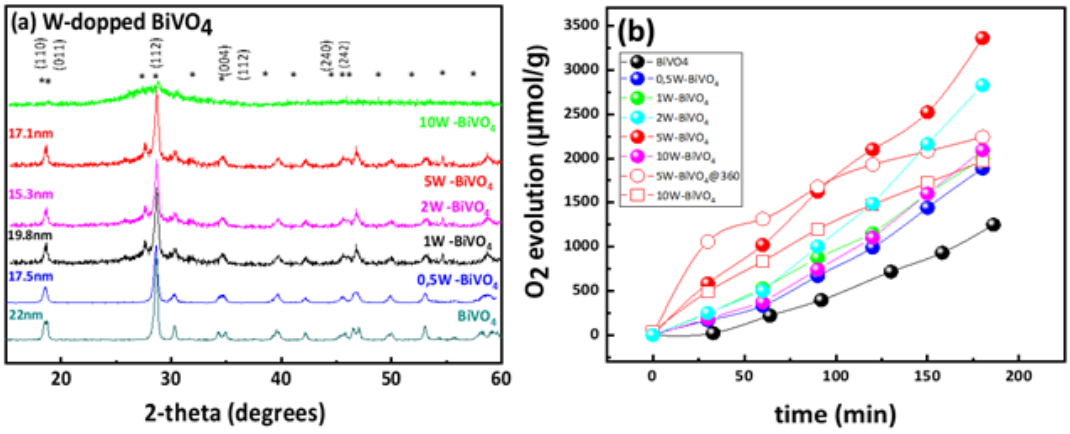

Figure 2. a) XRD patterns of the FSP-made W-doped $BiVO_4$ nanoparticles**. b)** Kinetics O_2 evolution of W doped photocatalysts compared to $BiVO_4$.

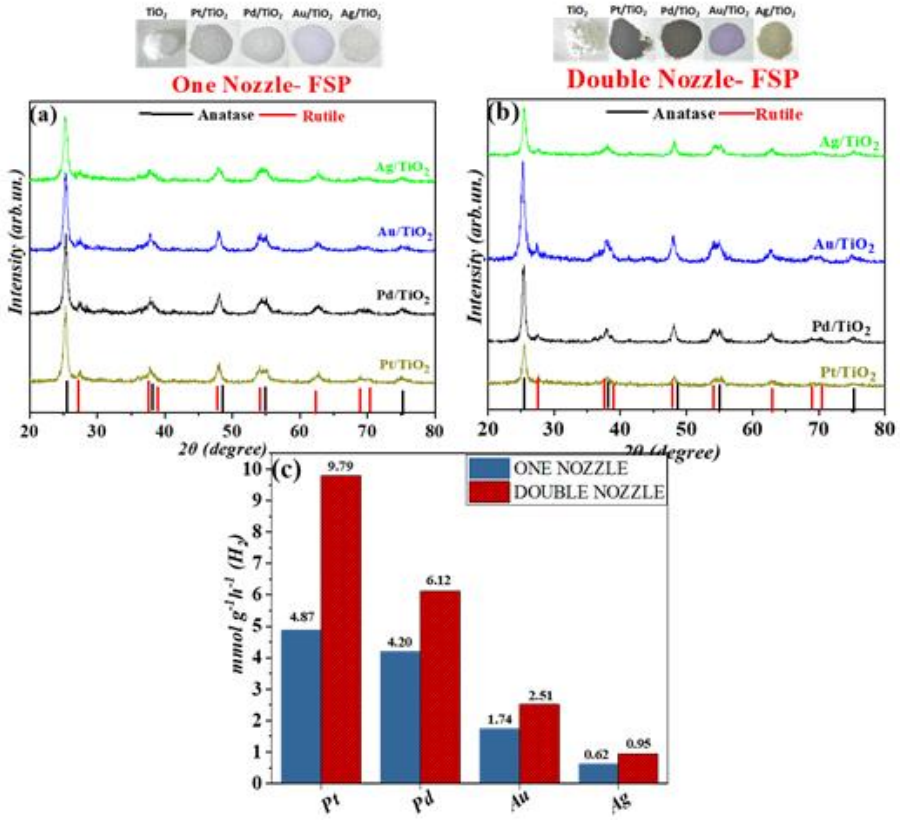

Figure 3. XRD patterns of **a)** One-Nozzle FSP and **b)** Double-Nozzle FSP 0.5% Pd-TiO_2 nanoparticles. **c)** Photocatalytic Hydrogen Production of N^0-TiO_2 nanoparticles.

This could be explained taking under consideration the work functions of Pt, Pd, Au Ag and TiO_2 (φ_{Pt}=5.65 *eV*, φ_{Pd}=5.30 *eV*, φ_{Au}=5.21 *eV*, φ_{Ag}=4.26 *eV*, φ_{TiO2}=4.20 *eV)*. It is well known that the larger the difference between the [metal work function] and [E_{CB} of TiO_2] the stronger the formed

Schottky barrier. Thus, in the case of Pt, the formed upward band bending is larger in the case of Pt, thus the electrons are trapped more efficiently in the conduction band of TiO_2.

As shown in Fig. 3c materials produced by DN-FSP exhibit by far better photocatalytic performance and even double their activity, in the case of Pt. This difference in the photocatalytic activity of nanomaterials engineered with DN-FSP vs. ON-FSP can be attributed to a series of reasons such as a) better dispersion of noble metal to the surface of TiO_2, b) smaller noble metal particle size, c) better {metal particle-oxide particle} adhesion. The synthesis process is of the utmost importance and could greatly affect photocatalytic performance[34]. Especially, in the case of gas-phase synthesis where FSP provides an easy and one-step process for the engineering of multicomponent and/or doped materials for catalytic applications the setup configuration plays a critical role[27].

An important and attractive feature of any synthesis process is its scalability while maintaining the physicochemical properties of the material. While wet-chemical methods show significant hurdles for scale-up, flame aerosol synthesis is an already scale-up process. Maintaining the physicochemical properties requires a proper and deep understanding of the process from both experimental and theoretical background.

Table 1. FSP made nanocatalysts for the photocatalytic production of O_2 and H_2 from H_2O and their equivalent catalytic yields.

Material	Synthesis	Source Of Irradiation	Catalytic Yield	Reference
Doped $BiVO_4$	One Nozzle FSP	125W Hg λ_{max} = 440 nm	O_2: 420 μmol g^{-1} h^{-1} ($BiVO_4$) O_2: 1074 μmol g^{-1} h^{-1} (5W-$BiVO_4$)	[19]
$BiVO_4$	Flame Synthesis of $BiVO_4$ and Acid Modification	300W Xe lamp with a 420 nm cut off filter	O_2: >300 μmol after 4h of illumination	[35]
Mullite $Bi_2Fe_4O_9$ Perovskite $BiFeO_3$	One Nozzle FSP and further annealing	125W Hg	O_2: 1150 μmol g^{-1} h^{-1} (T_{anneal} = 550 °C, t_{anneal}=5min) ($BiFeO_3$), 1300 μmol g^{-1} h^{-1} (T_{anneal} = 625 °C, t_{anneal}=60min) (1:1 $BiFeO_3$:$Bi_2Fe_4O_9$), 1550 μmol g^{-1} h^{-1} (T_{anneal} = 700 °C, t_{anneal}=60min) ($Bi_2Fe_4O_9$)	[17]
NM^0-TiO_2 (NM^0 = Pt^0, Pd^0, Au^0, Ag^0)	One Nozzle FSP	300W Xe lamp	H_2: 0.62 mmol g^{-1} h^{-1} (Ag^0), 1.74 mmol g^{-1} h^{-1} (Au^0), 4.2 mmol g^{-1} h^{-1} (Pd^0), 4.87 mmol g^{-1} h^{-1} (Pt^0)	[20]
	Double Nozzle FSP		H_2: 0.95 mmol g^{-1} h^{-1} (Ag^0), 2.51 mmol g^{-1} h^{-1} (Au^0), 6.12 mmol g^{-1} h^{-1} (Pd^0), 9.79 mmol g^{-1} h^{-1} (Pt^0)	
0.1Pt/TiO_2	One Nozzle FSP	300W Xe lamp	H_2: 552.39 μmol h^{-1}	[36]
CuO_x / TiO_2	One Nozzle FSP	300W Xe lamp	H_2: 112.6 μmol h^{-1}	[37]
TiO_2 (39% Anatase)	One Nozzle FSP	300W Xe lamp	H_2: 425 μmol h^{-1}	[38]
Cu/Pt-containing TiO_2	One Nozzle FSP	300W Xe lamp	H_2: 22.7 mmol g^{-1} h^{-1}	[39]

Although FSP-made nanomaterials find application in many fields, in the field of catalysis and especially for the photocatalytic production of O_2 and H_2 from H_2O there is research that needs to be

made. Table 1 has a summary of the FSP-made photocatalytic nanoparticles that were used for the production of O_2 and H_2 from H_2O as well as their catalytic yields, the source of irradiation, and the FSP synthesis method.

Summary

Flame Spray Pyrolysis as an industrial technique offers a versatile scalable technology for the synthesis of nanosized semiconducting materials with distinct characteristics. In the present work, we have employed the FSP process for the synthesis of W-doped $BiVO_4$ and NM^0/TiO_2 nanocatalysts which demonstrate efficient O_2 and H_2 production from the photocatalytic conversion of H_2O respectively. Both $BiVO_4$ and TiO_2 are excellent examples of how an industrial technology can contribute to the field of photocatalysis and the economic impact it may have as a scalable process since it allows the fabrication of nanoparticles at a rate of kg/h. $BiVO_4$ is a benchmark oxygen-evolving nanocatalyst alongside RuO_2 and IrO_2 with a huge advantage, its low cost. Improving its overall photocatalytic performance using hetero-atoms (dopants) while maintaining the crystal structure brings a new perspective to the design of Z-scheme photocatalysts. TiO_2 on the other hand is one the most studied and well-known semiconducting materials with excellent chemical stability and performance which displays impressive results in the photocatalytic H_2 production. The present data demonstrate that DN-FSP allows one-step engineering of finely dispersed nano photocatalysts with very low noble metal loadings i.e., 0.5% are optimal for the photocatalytic performance.

Acknowledgments

This research was funded by the Hellenic Foundation for Research and Innovation (H.F.R.I) under the “First Call for H.F.R.I Research Projects to support Faculty members and Researchers and the procurement of high-cost research equipment grant” (HFRI-FM17-1888).

References

[1] A. Fujishima, K. Honda, *Nature* **1972**, *238*, 37–38.

[2] J. Zhong, X. Yang, Z. Wu, B. Liang, Y. Huang, T. Zhang, *Chem. Soc. Rev.* **2020**, *49*, 1385–1413.

[3] C. Chen, W. Ma, J. Zhao, *Chem. Soc. Rev.* **2010**, *39*, 4206–4219.

[4] K. Sivula, R. Van De Krol, *Nat. Rev. Mater.* **2016**, *1*, DOI 10.1038/natrevmats.2015.10.

[5] B. Zhang, L. Sun, *Chem. Soc. Rev.* **2019**, *48*, 2216–2264.

[6] E. Pratsinis, **1998**, *24*, 197–219.

[7] S. Magdassi, A. Bassa, Y. Vinetsky, A. Kamyshny, *Chem. Mater.* **2003**, *15*, 2208–2217.

[8] A. Errokh, A. Magnin, J. L. Putaux, S. Boufi, *Mater. Sci. Eng. C* **2019**, *105*, DOI 10.1016/J.MSEC.2019.110044.

[9] W. Y. Teoh, R. Amal, L. Mädler, *Nanoscale* **2010**, *2*, 1324–1347.

[10] R. Jossen, M. C. Heine, S. E. Pratsinis, S. M. Augustine, M. K. Akhtar, *Appl. Catal. B Environ.* **2007**, *69*, 181–188.

[11] J. R. Jensen, T. Johannessen, S. Wedel, H. Livbjerg, *J. Catal.* **2003**, *218*, 67–77.

[12] L. Belles, C. Moularas, S. Smykała, Y. Deligiannakis, *Nanomaterials* **2021**, *11*, 925.

[13] E. Campagnoli, A. Tavares, L. Fabbrini, I. Rossetti, Y. A. Dubitsky, A. Zaopo, L. Forni, *Appl. Catal. B Environ.* **2005**, *55*, 133–139.

[14] C. Oliva, L. Bonoldi, S. Cappelli, L. Fabbrini, I. Rossetti, L. Forni, *J. Mol. Catal. A Chem.* **2005**, *226*, 33–40.

[15] R. Strobel, W. J. Stark, L. Mädler, S. E. Pratsinis, A. Baiker, *J. Catal.* **2003**, *213*, 296–304.

[16] P. Psathas, Y. Georgiou, C. Moularas, G. S. Armatas, Y. Deligiannakis, *Powder Technol.* **2020**, *368*, 268–277.

[17] P. Psathas, M. Solakidou, A. Mantzanis, Y. Deligiannakis, *Energies* **2021**, *14*, DOI 10.3390/en14175235.

[18] W. J. Stark, J. D. Grunwaldt, M. Maciejewski, S. E. Pratsinis, A. Baiker, *Chem. Mater.* **2005**, *17*, 3352–3358.

[19] P. Stathi, M. Solakidou, Y. Deligiannakis, *Nanomaterials* **2021**, *11*, 1–15.

[20] M. Solakidou, Y. Georgiou, Y. Deligiannakis, *Energies* **2021**, *14*, 1–16.

[21] G. D. Ulrich, *Combust. Sci. Technol.* **1971**, *4*, 47–57.

[22] M. Sokolowski, A. Sokolowska, A. Michalski, B. Gokieli, *J. Aerosol Sci.* **1977**, *8*, 219–230.

[23] A. Kilian, T. F. Morse, *Aerosol Sci. Technol.* **2001**, *34*, 227–235.

[24] L. Mädler, H. K. Kammler, R. Mueller, S. E. Pratsinis, *J. Aerosol Sci.* **2002**, *33*, 369–389.

[25] R. Mueller, L. Mädler, S. E. Pratsinis, *Chem. Eng. Sci.* **2003**, *58*, 1969–1976.

[26] R. Koirala, S. E. Pratsinis, A. Baiker, *Chem. Soc. Rev.* **2016**, *45*, 3053–3068.

[27] S. Pokhrel, L. Mädler, *Energy and Fuels* **2020**, *34*, 13209–13224.

[28] M. Høj, D. K. Pham, M. Brorson, L. Mädler, A. D. Jensen, J. D. Grunwaldt, *Catal. Letters* **2013**, *143*, 386–394.

[29] M. Minnermann, H. K. Grossmann, S. Pokhrel, K. Thiel, H. Hagelin-Weaver, M. Bäumer, L. Mädler, *Catal. Today* **2013**, *214*, 90–99.

[30] M. Tepluchin, D. K. Pham, M. Casapu, L. Mädler, S. Kureti, J. D. Grunwaldt, *Catal. Sci. Technol.* **2015**, *5*, 455–464.

[31] J. Horlyck, S. Pokhrel, E. Lovell, N. M. Bedford, L. Mädler, R. Amal, J. Scott, *Catal. Sci. Technol.* **2019**, *9*, 4970–4980.

[32] E. C. Lovell, H. Großman, J. Horlyck, J. Scott, L. Mädler, R. Amal, *ACS Appl. Mater. Interfaces* **2019**, *11*, 25766–25777.

[33] R. Strobel, A. Baiker, S. E. Pratsinis, *Adv. Powder Technol.* **2006**, *17*, 457–480.

[34] X. Jiang, X. Fu, L. Zhang, S. Meng, S. Chen, *J. Mater. Chem. A* **2015**, *3*, 2271–2282.

[35] Y. K. Kho, W. Y. Teoh, A. Iwase, † Lutz, M. Adler, A. Kudo, R. Amal, *ACS Appl. Mater. Interfaces* **2011**, *3*, DOI 10.1021/am200247y.

[36] F. Gao, Z. Xu, H. Zhao, in *Proc. Combust. Inst.*, Elsevier, **2021**, pp. 6503–6511.

[37] F. Yang, M. Liu, X. Chen, Z. Xu, H. Zhao, *Sol. RRL* **2018**, *2*, DOI 10.1002/solr.201800215.

[38] Y. K. Kho, A. Iwase, W. Y. Teoh, L. Mädler, A. Kudo, R. Amal, *J. Phys. Chem. C* **2010**, *114*,

2821–2829.

[39] M. Bernareggi, M. V. Dozzi, L. G. Bettini, A. M. Ferretti, G. L. Chiarello, E. Selli, *Catal. 2017, Vol. 7, Page 301* **2017**, *7*, 301.